HOKKAIDO UNIVERSITY

Title	Ice speed of a calving glacier modulated by small fluctuations in basal water pressure
Author(s)	Sugiyama, Shin; Skvarca, Pedro; Naito, Nozomu; Enomoto, Hiroyuki; Tsutaki, Shun; Tone, Kenta; Marinsek, Sebastián; Aniya, Masamu
Citation	Nature Geoscience, 4(9), 597-600 https://doi.org/10.1038/ngeo1218
Issue Date	2011-09
Doc URL	http://hdl.handle.net/2115/48493
Type	article (author version)
File Information	NG4-9_597-600.pdf

Instructions for use

Hokkaido University Collection of Scholarly and Academic Papers : HUSCAP

Ice speed of a calving glacier modulated by small fluctuations in basal water pressure

Shin Sugiyama[1*], Pedro Skvarca[2], Nozomu Naito[3], Hiroyuki Enomoto[4], Shun Tsutaki[1,5], Kenta Tone[1,5], Sebastián Marinsek[2], Masamu Aniya[6]

[1]Institute of Low Temperature Science, Hokkaido University, Nishi8, Kita19, Sapporo, Japan
[2]Instituo Antártico Argentino, Cerrito 1248, 1010 Buenos Aires, Argentina
[3]Hiroshima Institute of Technology, 2-1-1 Miyake, Saeki-ku, Hiroshima, Japan
[4]Kitami Institute of Technology, 165 Koen-cho, Kitami, Japan
[5]Graduate School of Environmental Science, Hokkaido University, Nishi5, Kita10, Sapporo, Japan
[6]Tsukuba University, 1-1-1 Tennodai, Tsukuba, Japan

[*]Please address e-mail correspondence to: sugishin@lowtem.hokudai.ac.jp

June 26, 2011

Ice flow acceleration has played a crucial role in the recent rapid retreat of calving glaciers in Alaska[1,2], as well as in Greenland and Antarctica[3,4]. Fast flow of such glaciers is due primarily to basal ice motion[5], but its mechanism is poorly understood because subglacial observations are scarce in calving glaciers. Here we show high-frequency ice speed and basal water pressure measurements performed in Glaciar Perito Moreno, a fast-flowing calving glacier in Patagonia. The water pressure was measured in a borehole drilled through the 515±5 m thick glacier at a site where more than 60% of ice is below the proglacial lake level. We found that mean basal water pressure reached 94–96% of the ice overburden pressure, and that a few percent of pressure changes were driving nearly 40% of ice speed variations. The ice speed was strongly correlated to air temperature, suggesting the glacier motion was modulated by water pressure

under the influence of changing meltwater input. Our observations demonstrate the great importance of basal water pressure in the calving glacier dynamics and its close connection to climate conditions. It is thus crucial to take into account the elevated basal water pressure for predicting future evolution of calving glaciers.

Acceleration of fast-flowing calving glaciers is the focus of attention as it is responsible for the rapid retreat of large tidewater glaciers in Alaska[1,2] as well as the recent wastage of Greenland and the Antarctic ice sheets[3,4]. Calving glaciers flow much faster than those terminating on land as a result of basal ice motion enhanced by high basal water pressure[5]. A commonly used basal flow law states

$$u_b = k\frac{{\tau_b}^p}{(P_i - P_w)^q} = k\frac{{\tau_b}^p}{{P_e}^q} \ , \tag{1}$$

where u_b is the basal ice speed, τ_b is the basal shear stress, P_i and P_w are ice overburden and basal water pressures, and k, p and q are empirical parameters[6,7]. Because τ_b is primarily controlled by ice thickness and surface slope, changes in basal water pressure play a critical role in short-term ice speed variations. Observations in mountain glaciers have shown rapid acceleration as basal water pressure approaches ice overburden pressure[8−10], which confirms the non-linear dependence of the basal ice speed on the effective pressure defined by $P_e = P_i - P_w$. The hydraulic head within a calving glacier is expected to be higher than the surface level of the proglacial water body, which maintains basal water pressure closer to ice overburden. According to the inverse proportionality of u_b to P_e, small perturbations in P_w near P_i result in large ice speed variations. Moreover, changes in P_i due to glacier thinning or thickening have a great impact on the ice speed as well. These characteristics make calving glacier dynamics more susceptible to external forcing than land terminating glaciers. Studying the response of ice speed to the changes in P_e is thus crucial for predicting the future evolution of calving glaciers. However, only a very few water pressure measurements have been performed in calving glaciers

and have never been reported in Patagonia.

The Patagonia Icefields cover an area of 1.70×10^4 km^2 (refs 11, 12), forming the second largest ice mass in the southern hemisphere. Most of the glaciers in Patagonia have been retreating and thinning for the last several decades[12,13], which contributes to a sea level rise of 0.042–0.105$\pm$0.011 mm a^{-1} (ref. 14). Warming climate is a likely cause of the ice loss[13], but changes in glacier dynamics is important as more than 80% of major outlet glaciers discharge ice into lakes and the ocean by calving[14,15]. Glaciar Perito Moreno (GPM) is one such glacier with a length of 30 km and an area of 258 km^2 situated in the southeast of the Southern Patagonia Icefield[13]. In the region extending 8 km from the terminus, approximately 50–70% of ice thickness is below the surface of proglacial lakes, Brazo Rico and Cannal de los Témpanos (Fig. 1) (ref. 16). In this region, ice speed is more than 400 m a^{-1} and the glacier is 200–800 m thick along the central flowline[16].

In the austral summer 2008/09 and 2010, we operated three GPS (Global Positioning System) receivers on GPM at hourly intervals to measure short-term ice speed variations and their relationship with air temperature and basal water pressure. The study site was 4.7 km from the terminus and the bed elevation was more than 380 m below the lake level[16] (Fig. 1). In March 2010, we drilled two boreholes with a hot-water drilling technique at 160 m south of GPS1 (ref. 17) (Fig. 1a). According to the length of the hose used for the drilling, ice thickness was 515$\pm$5 m. Water level in the boreholes dropped before the drill reached the bed, which occurred at depths of 176 and 344 m for the first drilling and at 375 m for the second. After the drilling, water level was measured every 10–30 min using pressure sensors suspended in the boreholes. Details of the measurements are described in the Methods section.

Ice speed showed diurnal and longer-term variations over the observation periods (Figs 2a and b). During the one-month measurement period in 2010, ice speed varied by $+71$ to -26% from the mean of 1.43 m d^{-1}. An intriguing feature is the strong correlation between the ice

speed and air temperature. Hourly ice speed correlated positively to the air temperature with a correlation coefficient $r = 0.76$ for the entire observation period (Fig. 2c and Supplementary Table S1). A maximum correlation was achieved when the ice speed lag was 1 h relative to the temperature (Supplementary Fig. S1). Linear regression indicates that the ice speed deviated ± 0.053 m d^{-1} for a temperature change of $\pm 1^{\circ}$C. A likely mechanism of the air-temperature-dependent ice speed variation was the change in basal water pressure driven by meltwater input. Melt production is commonly related to the positive degree day (ref. 18) as we observed at GPM (Supplementary Information and Fig. S2).

From 4 to 13 March 2010, mean water levels in the boreholes were 440 (BH1) and 450 m (BH1) above the bed, i.e., 110–120 m higher than the proglacial lake level (Figs 1b and 3a). This observation indicated that the basal water pressure was at 94–96% of the ice overburden pressure and effective pressure was only 190–280 kPa. The water level oscillated in a diurnal manner with an amplitude of 10–15 m from 5 to 10 March (Fig. 3a). The levels were not exactly the same in the two boreholes, but the oscillations were in phase. The ice speed at GPS1 and GPS2 was correlated to the water level (Figs 3a–c). The range of the ice speed variation was 37% of the mean at GPS1, whereas that of the water level was only 4–6% (Fig. 3c).

The borehole data show that the glacier bed is exposed to consistently high water pressure, and large diurnal ice speed variations are driven by small pressure fluctuations near the ice overburden. These observations are consistent with equation (1), which relates the basal ice speed to the inverse power of effective pressure. A numerical ice flow model shows that 94% of the observed ice speed at GPS1 is due to basal ice motion (Supplementary Information and Fig. S3). Thus, we neglected the contribution of internal ice deformation to the total glacier motion, and performed the fitting of equation (1) to the ice speed (GPS1) and pressure (mean of BH1 and BH2) data to find the dependence of basal ice speed on the effective pressure. The least square fitting yields

$$u_b = 0.91\ {P_e}^{-0.35} \qquad \sigma = 0.061\ , \tag{2}$$

where u_b and the root mean square error σ are in m d^{-1} and P_e is in MPa (Supplementary Table S2). The fitting curve clearly indicates that the basal ice speed of GPM is highly dependent on the effective pressure within the observed pressure range (Fig. 3d).

Water pressure beneath a calving glacier was previously measured at Columbia Glacier, an Alaskan tidewater glacier with dimensions similar to those of GPM (about 5 km wide and 400–1000 m thick). Basal water pressure was consistently high and the effective pressure varied within a range of -100 and 300 kPa (ref. 19). These figures are similar to those we observed at GPM, but ice speed at Columbia Glacier was not well correlated with water pressure nor with air temperature. It was argued that basal pressure was non-uniformly distributed and the borehole measurements did not represent spatially averaged pressure which is more important for ice speed variations[20]. It is assumed that horizontal patterns of subglacial hydraulic conditions at Columbia Glacier are less uniform than those at GPM, as described below.

Our observation revealed a clear relationship between air temperature and ice speed, which implies that basal water pressure is controlled primarily by the meltwater production rate. However, previous studies showed that basal pressure is not simply a function of water input, but that is substantially influenced by the evolution of subglacial drainage conditions over a time scale of days to months[10,21]. For example, a melt event in the early ablation season elevates basal pressure, resulting in a speed-up event[22,23]. The speed-up ceases as a drainage system develops and water drains downglacier more efficiently. Moreover, the response of basal pressure to surface melt is often delayed more than several hours[10]. At GPM, the consistently high correlation between the ice speed and the air temperature suggests a swift transfer of surface meltwater to the basal hydraulic system and a relatively constant drainage efficiency. Presumably, the meltwater immediately drains into crevasses which cover most part of the glacier, and

it reaches the hydraulic system within a short time since hydraulic head is only 60–80 m below the surface. High water pressure and a large amount of meltwater input all year round[16] are favorable conditions for maintaining the drainage systems in a more uniform way as compared with other glaciers. Spatially uniform drainage system configurations are suggested by other observations: the englacial drainage of the borehole water during the drilling, very similar water level variations in the two boreholes and synchronous ice speed variations at GPS1 and GPS2. These observations contrast to those reported for other glaciers, which suggested non-uniformly distributed subglacial hydraulic conditions[24,25].

The observations in GPM have important implications for studying the dynamic behaviour of calving glaciers. First, the borehole levels were significantly higher than the lake level, which disagrees with a common assumption that equates subglacial hydraulic head to the surface of proglacial water body[26]. This is crucial, as the ice speed is highly underestimated with such an assumption. Second, we confirmed that the calving glacier dynamics are very sensitive to small basal water pressure variations near the ice overburden. Together with the close correlation of the ice speed with the air temperature, calving glaciers are assumed to be very susceptible to changing climate. If the ice speed increases under the rising air temperature condition, ice dissipation by calving increases, causing thinning of the glacier. The thinning in turn reduces the effective pressure, which results in further acceleration of the glacier[5,27]. According to equation (1), basal ice speed in GPM is negatively correlated with ice thickness under the observed basal water pressure condition (Supplementary Information and Fig. S4).

Recent studies using numerical models reproduced several aspects of dynamic behaviour of outlet glaciers in Greenland by capturing calving processes[28]. However, basal water pressure is not well imposed in the model as described above. The foregoing discussion suggests a positive feedback effect between thinning and acceleration of calving glaciers, which can be captured by modelling only with realistic basal water pressure and an effective pressure dependent basal

flow law. Further investigations of subglacial processes and accurate treatment of basal conditions in a model are thus crucial for predicting the future evolution of calving glaciers in Patagonia and Alaska, as well as marine-terminating outlet glaciers in Greenland and Antarctica.

Methods

Ice speed was measured at GPS1–3 (Fig. 1a) with dual frequency GPS receivers (Leica System 1200) from 27 December 2008 to 8 January 2009 and from 25 February to 2 April 2010. We installed 2-m-long aluminum poles in the ice and mounted GPS antennae at the top of the poles. The GPS receivers were activated every hour for 30 min and the satellite signals were processed with data recorded at a reference GPS station fixed on a stable rock on a side moraine (Fig. 1a). A GPS processing software (Leica Geo Office) was used to obtain stake positions with an accuracy of 3–5 mm (ref. 10). We computed horizontal ice speed after smoothing the data with a Gaussian filter having a bandwidth of 1.5 hours. This bandwidth was chosen so that the mean deviation of the data from the smoothed curve was equivalent to the positioning accuracy. The relative error in the computed hourly ice speed was 7–12% for the mean speed at GPS1, and the actual error after the smoothing procedure was smaller than this estimate.

Boreholes were drilled by means of a hot-water drilling system consisting of two high-pressure hot-water machines (Kärcher HDS1000BE) at a mean drilling rate of 49 m h^{-1} (ref. 17). The weight of the drilling hose was monitored during the drilling to detect the glacier bed. The ice thickness was determined as 515$\pm$5 m from the length of the hose used for the drilling and its extension due to own weight. Water levels in the boreholes BH1 and BH2 were measured with water pressure sensors (Geokon 4500S and HOBO U20-001-03) installed at 98 ± 1 and 120 ± 0.1 m from the surface, respectively. The measurement ranges/accuracies of the sensors

were -0.1–2 MPa/± 200 mm (BH1) and 0–0.85 MPa/± 38 mm (BH2). The pressure data were corrected for atmospheric pressure recorded every hour at the air temperature measurement site. The data availability was limited to 4–12 March at BH1 as the borehole was isolated from the subglacial drainage network afterwards, and 5–13 March at BH2, as we could not retrieve the data after the sensor got stuck in the borehole.

Air temperature was measured near the glacier front at the shore of Brazo Rico (Fig. 1a). A temperature sensor (Vaisala, HMP35AC) protected with a non-aspirated radiation shield was installed on a mast at 2 m above a rock surface. The temperature was measured every 10 seconds with an accuracy of ± 0.4°C to record hourly mean values in a datalogger (Campbell, 21X) (ref. 29).

References

1. Krimmel, R. M. Photogrammetric data set, 1957–2000, and bathymetric measurements for Columbia Glacier, Alaska. *U.S. Geol. Surv. Water Resour. Invest. Rep.* 01-4089, (2001).

2. O'Neel, S., Echelmeyer, K. A. & Motyka, R. J. Short-term flow dynamics of a retreating tidewater glacier: LeConte Glacier, Alaska, U.S.A.. *J. Glaciol.* **47**, 567–578 (2001).

3. Rignot, E. & Kanagaratnam P. Changes in the velocity structure of the Greenland ice sheet. *Science* **311**, 986–990 (2006).

4. Pritchard, H. D., Arthern, R. J., Vaughan, D. G. & Edwards, L. A. Extensive dynamic thinning on the margins of the Greenland and Antarctic ice sheets. *Nature* **461**, 971–975 (2009).

5. Meier, M. F. & Post, A. Fast tidewater glaciers. *J. Geophys. Res.* **92**(B9), 9051–9058 (1987).

6. Greve, R. & Blatter H. *Dynamics of Ice Sheets and Glaciers*, (Springer, 2009)

7. Bindschadler, R. The importance of pressurized subglacial water in separation and sliding at the glacier bed. *J. Glaciol.* **47**, 3–19 (1983).

8. Iken, A. & Bindschadler, R. A. Combined measurements of subglacial water pressure and surface velocity of Findelengletscher, Switzerland: conclusions about drainage system and sliding mechanism. *J. Glaciol.* **32**, 28–47 (1986).

9. Jansson, P. Water pressure and basal sliding on Storglaciären, northern Sweden. *J. Glaciol.* **41**, 232–240 (1995).

10. Sugiyama, S. & Gudmundsson, G. H. Short-term variations in glacier flow controlled by subglacial water pressure at Lauteraargletscher, Bernese Alps, Switzerland. *J. Glaciol.* **50**, 353–362 (2004).

11. Aniya, M., Naruse, R., Shizukuishi, M. Skvarca, P. & Casassa, G. Monitoring recent glacier variations in the Southern Patagonia Icefield, utilizing remote sensing data. *Int. Arch. Photogram. Rem. Sens.* **29**, 87–94 (1992).

12. Rivera, A., Benham, T., Casassa, G., Bamber, J. & Dowdeswell, J. A. Ice elevation and areal changes of glaciers from the Northern Patagonia Icefield, Chile. *Global Planet. Change* **59**, 126–137 (2007).

13. Aniya, M., Sato, H., Naruse, R., Skvarca, P. & Casassa, G. Recent glacier variations in the Southern Patagonia Icefield, South America. *Arct. Alp. Res.* **29**, 1–12 (1997).

14. Rignot, E., Rivera, A. & Casassa, G. Contribution of the Patagonia Icefields of South America to sea level rise. *Science* **302**, 434–437 (2003).

15. Warren, C. R. & Aniya, M. The calving glaciers of southern South America. *Global Planet. Change* **22**, 59–77 (1999).

16. Stuefer, M., Rott, H. & Skvarca, P. Glaciar Perito Moreno, Patagonia: climate sensitivities and glacier characteristics preceding the 2003/04 and 2005/06 damming events. *J. Glaciol.* **53**, 3–16 (2007).

17. Sugiyama, S. *et al.* Hot-water drilling at Glaciar Perito Moreno, Southern Patagonia Icefield. *Bulletin of Glaciological Research* **28**, 27–32 (2010).

18. Ohmura, A. Physical basis for the temperature-based melt-index method. *J. Appl. Meteorol.* **40**(4), 753–761 (2001).

19. Meier, M. F. *et al.* Mechanical and hydrologic basis for the rapid motion of a large tidewater glacier: 1. Observations. *J. Geophys. Res.* **99**(B8), 15219–15229 (1994).

20. Kamb, B. *et al.* Mechanical and hydrologic basis for the rapid motion of a large tidewater glacier: 2. Interpretation. *J. Geophys. Res.* **99**(B8), 15231–15244 (1994).

21. Gordon, S. *et al.* Seasonal reorganization of subglacial drainage inferred from measurements in boreholes. *Hydrol. Processes* **12**, 105–133 (1998).

22. Iken, A., Röthlisberger, H., Flotron, A. & Haeberli, W. The uplift of Unteraargletscher at the beginning of the melt season − a consequence of water storage at the bed? *J. Glaciol.* **29**, 28–47 (2001).

23. Mair, D., Nienow, P., Willis, I. & Sharp, M. Spatial patterns of glacier motion during a high-velocity event: Haut Glacier d'Arolla, Switzerland. *J. Glaciol.* **47**, 9–20 (2001).

24. Murray, T. & Clarke, G. K. C. Black-box modeling of the subglacial water system. *J. Geophys. Res.* **100**(B6), 10231–10245 (1995).

25. Nienow, P. W. *et al.* Hydrological controls on diurnal ice flow variability in valley glaciers. *J. Geophys. Res.* **110**, F04002, 15231–15244 (2005).

26. Vieli, A., Funk, M. & Blatter, H. Flow dynamics of tidewater glaciers: A numerical modelling approach. *J. Glaciol.* **47**, 595–606 (2001).

27. Pfeffer, W. T. A simple mechanism for irreversible tidewater glacier retreat. *J. Geophys. Res.* **112**, F03S25, (2007).

28. Nick, F. M., Vieli, A., Howat, I. M. & Joughin, I. Large-scale changes in Greenland outlet glacier dynamics triggered at the terminus. *Nature Geosci.* **2**, 110–114 (2009).

29. Stuefer, M. Investigations on mass balance and dynamics of Moreno Glacier based on field measurements and satellite imagery. (PhD thesis, University of Innsbruck, 1999).

Supplementary Information

Supplementary Information is provided as an additional file.

Author Information

Correspondence and requests for materials should be addressed to Shin Sugiyama (sugishin@lowtem.hokudai.ac.jp).

Acknowledgements

We thank the members of the field campaign at Glacier Perito Moreno in 2008/2009 and 2010 for their help on the glacier. Hielo y Aventura S. A. offered logistic support and Gendarmeria Nacional Argentina operated helicopter transportation. Drilling equipment was constructed by the workshop of the Institute of Low Temperature Science, Hokkaido University. Thanks are extended to R. Greve and H. Blatter for comments on the manuscript. This research was funded by the Japanese Ministry of Education, Science, Sports and Culture, Grant-in-Aid 18251002 (2005–2010) and 23403006 (2011–2014).

Author Contributions

S.S., P.S. and M.A. designed the research. S.S., N.N., H.E. and K.T. drilled the boreholes. S.S., P.S., N.N., S.T., K.T. and S.M. collected the water pressure and GPS data. S.S. analyzed the data and wrote the manuscript. The authors discussed the results and commented on the manuscript jointly.

Figure Captions

Fig. 1. Satellite image and longitudinal cross section of Glaciar Perito Moreno. (a) GPS (•, ○), drilling (+) and air temperature measurement (box) sites are indicated with ice flow vectors measured from 31 December 2008 to 7 January 2009. The image was taken on 27 March 2002 (image courtesy of the Image Science & Analysis Laboratory, NASA Johnson Space Center). (b) The bed profile is drawn by interpolation of observational data points (○) (ref. 16). Mean borehole water level during the measurement period is indicated.

Fig. 2. Ice speed and air temperature measured in 2008/09 and 2010 austral summer seasons. (a) Ice speed at GPS1 (black) and air temperature (red) obtained by filtering hourly data (grey). (b) Scatter plot of hourly ice speed and air temperature for the measurements in 2008/09 (blue) and 2010 (red).

Fig. 3. Ice speed and borehole water levels. (a) Water levels relative to the bed in BH1 (blue) and BH2 (red) for two different scales. Dashed lines indicate ice overburden (P_i) and lake levels (P_{lake}) in the left axis. (b) Ice speed at GPS1–3 (black) and air temperature (red). (c) Hourly ice speed at GPS1 v.s. water level in BH1 (blue) and BH2 (red) with curves obtained by fitting equation (1) to the data (Supplementary Table S2). (d) Ice speed v.s. effective pressure with a fitting curve that represents equation (2). Dashed lines indicate the effective pressures for water levels equal to zero ($P_e = P_i$) and to the lake surface ($P_e = P_i - P_{lake}$).

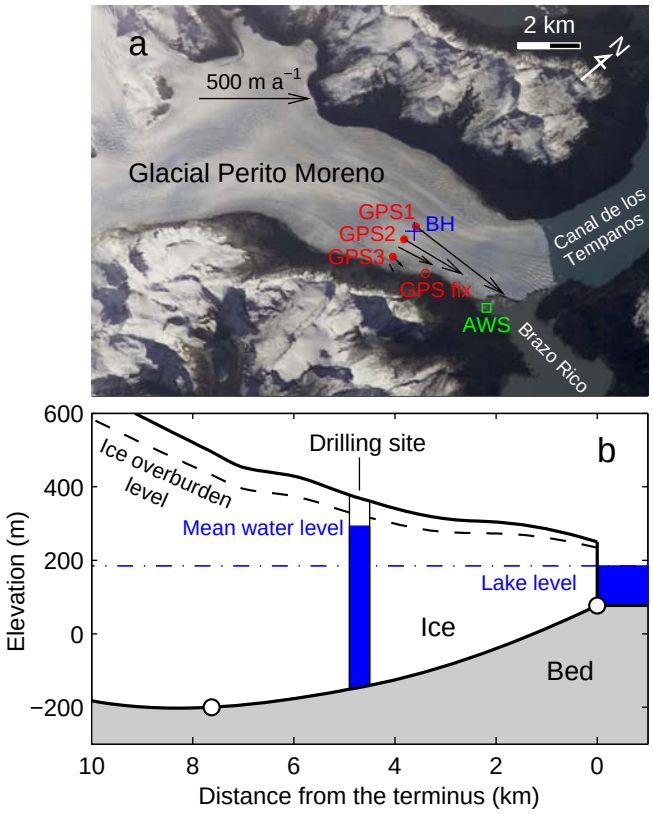
a
2 km
N
500 m a^{-1}
Glacial Perito Moreno
GPS1
GPS2
GPS3
BH
GPS fix
AWS
Canal de los Tempanos
Brazo Rico
b
Drilling site
Ice overburden level
Mean water level
Lake level
Ice
Bed
Elevation (m)
600
400
200
0
−200
10
8
6
4
2
0
Distance from the terminus (km)

Fig. 1

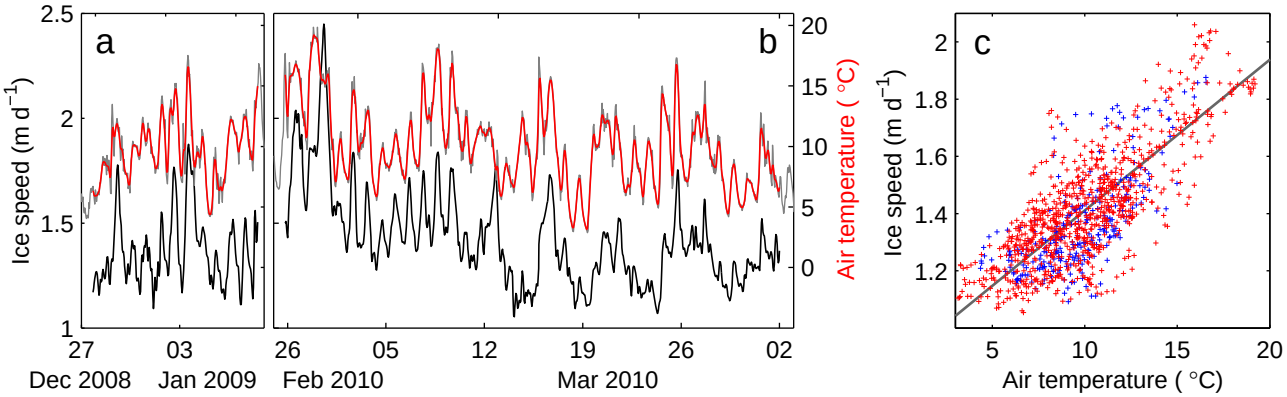
a
b
c
Ice speed (m d^{-1})
Air temperature (°C)
2.5
2
1.5
1
20
15
10
5
0
27
03
26
05
12
19
26
02
Dec 2008
Jan 2009
Feb 2010
Mar 2010
1.8
1.6
1.4
1.2
5
10
15
20

Fig. 2

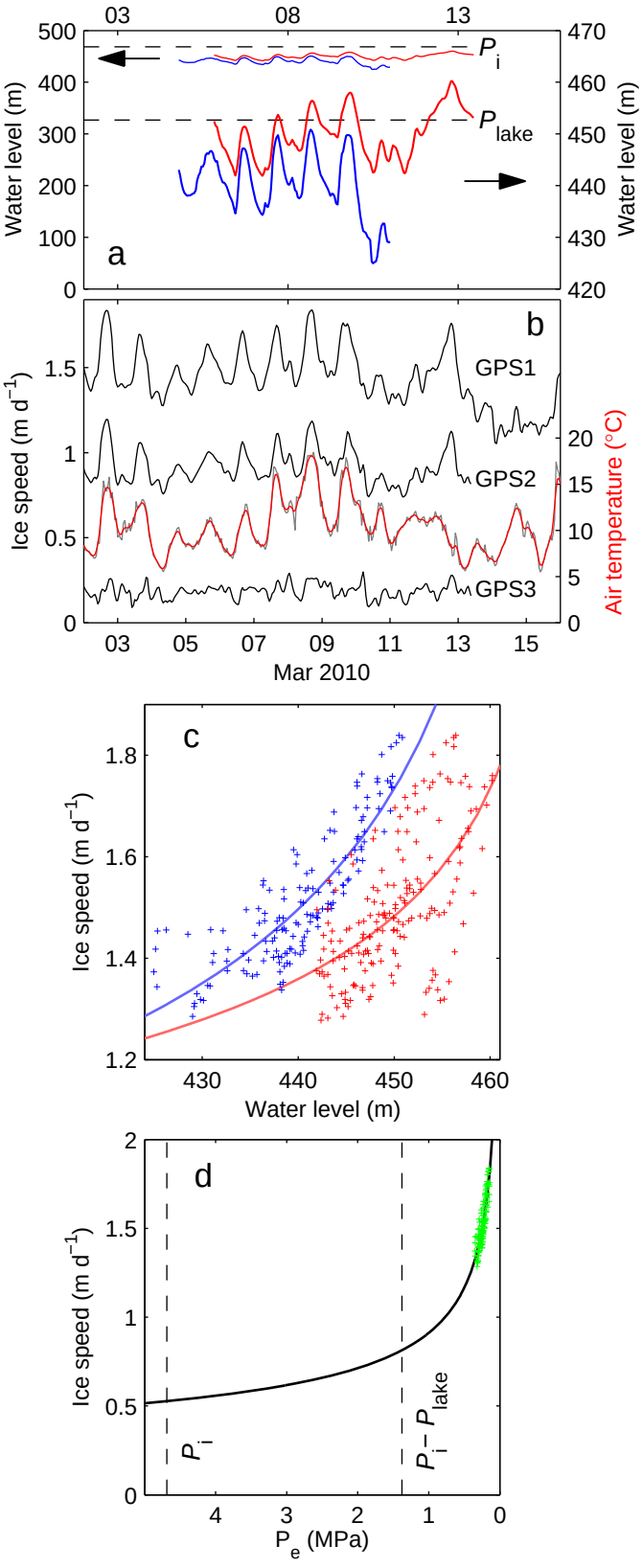
03
08
13
500
400
300
200
100
0
470
460
450
440
430
420
Water level (m)
Water level (m)
P_i
P_{lake}
a
b
GPS1
GPS2
GPS3
Ice speed (m d^{-1})
1.5
1
0.5
0
20
15
10
5
0
Air temperature (°C)
03
05
07
09
11
13
15
Mar 2010
c
1.8
1.6
1.4
1.2
Ice speed (m d^{-1})
430
440
450
460
Water level (m)
d
2
1.5
1
0.5
0
Ice speed (m d^{-1})
P_i
$P_i - P_{lake}$
4
3
2
1
0
P_e (MPa)

Fig. 3

Supplementary information
"Ice speed of a calving glacier modulated by small fluctuations in basal water pressure"

Shin Sugiyama[1*], Pedro Skvarca[2], Nozomu Naito[3], Hiroyuki Enomoto[4], Shun Tsutaki[1,5], Kenta Tone[1,5], Sebastián Marinsek[2], Masamu Aniya[6]

[1]Institute of Low Temperature Science, Hokkaido University, Nishi8, Kita19, Sapporo, Japan
[2]Instituo Antártico Argentino, Cerrito 1248, 1010 Buenos Aires, Argentina
[3]Hiroshima Institute of Technology, 2-1-1 Miyake, Saeki-ku, Hiroshima, Japan
[4]Kitami Institute of Technology, 165 Koen-cho, Kitami, Japan
[5]Graduate School of Environmental Science, Hokkaido University, Nishi5, Kita10, Sapporo, Japan
[6]Tsukuba University, 1-1-1 Tennodai, Tsukuba, Japan

*Please address e-mail correspondence to: sugishin@lowtem.hokudai.ac.jp

1 Ice surface melt

Ice surface melt was measured at GPS1 and GPS2 (Fig. 1a). The length of the GPS survey poles above the ice surface was recorded once or twice a day, and the error in the measurement due to ice surface roughness was about ± 10 mm. The sum of the positive degree day (PDD) was computed from the air temperature measured near the terminus (Fig. 1a), assuming a lapse rate of 0.0061 °C m^{-1}. This lapse rate is based on two-year temperature records in 2009 and 2010 at the AWS used in this study and at 1236 m a.s.l. on the southern flank of the glacier. Linear regression of accumulated melt to the sum of PDD resulted in a linear coefficient (PDD factor) of 4.0 mm w.e. °C^{-1} d^{-1} with a correlation coefficient 0.98 and a p-value $< 10^{-6}$ (Fig. S2). Stuefer[S1] reported a lapse rate of 0.0124 °C m^{-1} from temperature measured at the AWS and on

the glacier within several hundred meters from GPS1 for 20 days in November and December 1996. The PDD factor based this lapse rate is 4.5 mm w.e. $^{\circ}\mathrm{C}^{-1}$ d^{-1}.

2 Estimation of basal ice speed

We estimated basal ice speed of Glaciar Perito Moreno by computing an englacial flow field using a two-dimensional finite-element ice flow model[S2]. An ice speed field within a transverse cross section was computed by solving the balance of shear stresses with a first order approximation[S3,S4] and Glen's flow law:

$$\frac{\partial \tau_{yx}}{\partial y} + \frac{\partial \tau_{zx}}{\partial z} = \rho_i g \sin\alpha \ , \tag{S1}$$

$$\dot{\varepsilon}_{ij} = A \tau_e^{n-1} \tau_{ij} \ , \tag{S2}$$

where τ_{ij} and $\dot{\varepsilon}_{ij}$ are the shear stress and strain rate; $\rho_i = 910$ kg m^{-3}, the ice density; $g = 9.8$ m s^{-2}, the gravitational acceleration; $A = 75$ MPa^{-3} a^{-1}, the rate factor[S5]; τ_e, the effective stress; and $n = 3$, the stress exponent. The surface slope $\sin\alpha = 0.032$ is a mean slope for the lower 8 km of the glacier based on the surface elevation data reported by Stuefer[S1]. Cartesian coordinates, x, y and z were taken downglacier, crossglacier and vertically upward, respectively. Basal ice speed was introduced as a linear function of the basal shear stress τ_b.

$$u_b = c(y)\tau_b \tag{S3}$$

Equations (S1) and (S2) were solved for downglacier ice speed u_x using the finite-element method, imposing equation (S3) as a boundary condition at the bed. The cross section of the glacier was discretized by 400 triangular elements as shown in Fig. S3a. Since bed elevation was available only for the southern half of the cross section along GPS1–3 (ref. S6), the modelled cross section was assumed to be symmetrical about the glacier center.

The coefficient $c(y)$ in equation (S3) was prescribed such that the computed surface ice speed reproduced the measurements at GPS1–3. We used mean ice speed from 31 December 2008 to 7 January 2009 for this purpose. Reasonable agreement with the field data was achieved as shown in Figs S3b and c. The computed ice speed shows that 94% of surface speed at GPS1 is due to basal ice motion. For this reason, we neglected the 6% contribution of ice deformation and fit equation (1) to the field data.

The model sensitivity to the bed geometry was studied by assuming two different bed profiles for the region where bed elevation is not known (blue curves in Fig. S3a). As the ice speed was influenced by the geometry change, the coefficient $c(y)$ had to be adjusted to achieve fitting to the field data. After the optimization of $c(y)$, the changes in the proportion of the basal to the surface ice speed was $+1.5/-0.5$% from that obtained for the symmetrical bed profile. In the same way, the sensitivity to a ± 10% surface slope change was calculated as $+3/-2$%.

3 Response of basal ice speed to ice thickness change

Equation (1) states that basal ice speed is dependent on ice thickness, because the basal shear stress τ_b and effective pressure P_i are functions of the thickness. By taking shallow ice approximation ($\tau_b = \rho g h \sin\alpha$) (ref. S4), differentiation of equation (1) with respect to ice thickness h produces

$$\begin{aligned}
\frac{\partial u_b}{\partial h} &= k\frac{\partial}{\partial h}\frac{{\tau_b}^p}{(P_i - P_w)^q} \\
&= k\frac{\partial}{\partial h}\frac{(\rho_i g h \sin\alpha)^p}{(\rho_i g h - P_w)^q} \\
&= k(\rho_i g \sin\alpha)^p h^{p-1}(P_i - P_w)^{-q-1}\{P_i(p-q) - pP_w\}. \qquad \text{(S4)}
\end{aligned}$$

Given $(P_i - P_w) > 0$, the derivative $\frac{\partial u_b}{\partial h}$ is negative under the condition

$$\frac{P_w}{P_i} > \frac{p-q}{p} \,. \tag{S5}$$

Thus, the basal ice speed increases as a result of ice thinning when the water pressure is higher than a critical value determined by the exponents p and q (refs S7, S8). Several different values have been proposed for p and q based on field data[S9,S10] as well as laboratory experiments[S11]. Among those reported, the most commonly accepted values are $p = 3$ and $q = 1$ (refs S4, S9). If we assume these values, the derivative is negative as long as the basal water pressure is greater than 66% of ice overburden pressure (Fig. S4). If we take the value of q in equation (2) ($q = 0.35$), the required water pressure is above 88% of the ice overburden. At our study site in Glaciar Perito Moreno, the pressure exceeds 90% of the overburden pressure, and thus the derivative is negative, i.e., basal ice speed is expected to increase as ice thickness decreases.

References

S1. Stuefer, M. Investigations on mass balance and dynamics of Moreno Glacier based on field measurements and satellite imagery. (PhD thesis, University of Innsbruck, 1999).

S2. Sugiyama, S., Bauder, A., Zahno, C. & Funk, M. Evolution of Rhonegletscher, Switzerland, over the past 125 years and in the future: application of an improved flowline model. *Ann. Glaciol.*, **46**, 268–274 (2007).

S3. Nye, J. F. The flow of a glacier in a channel of rectangular, elliptic or parabolic cross-section. *J. Glaciol.* **5**(41), 661–690 (1965).

S4. Greve, R. & Blatter H. *Dynamics of Ice Sheets and Glaciers*, (Springer, 2009)

S5. Gudmundsson, G. H. A three-dimensional numerical model of the confluence area of Unteraargletscher, Bernese Alps, Switzerland. *J. Glaciol.* **45**(150), 219–230 (1999).

S6. Stuefer, M., Rott, H. & Skvarca, P. Glaciar Perito Moreno, Patagonia: climate sensitivities and glacier characteristics preceding the 2003/04 and 2005/06 damming events. *J. Glaciol.* **53**, 3–16 (2007).

S7. O'Neel S. & Pfeffer, W. T. Evolving force balance at Columbia Glacier, Alaska, during its rapid retreat. *J. Geophys. Res.* **110**, F03012 (2005).

S8. Pfeffer, W. T. A simple mechanism for irreversible tidewater glacier retreat. *J. Geophys. Res.* **112**, F03S25 (2007).

S9. Bindschadler, R. The importance of pressurized subglacial water in separation and sliding at the glacier bed. *J. Glaciol.* **29**(101), 3–19 (1983).

S10. Lingle, C. S. & Brown, T. J. A subglacial aquifer bed model and water pressure dependent basal sliding relationship for a west Antarctic ice stream. *In* van der Veen, C. J. and J. Oerlemans (eds.), *Dynamics of the West Antarctic Ice Sheet*, Reidel Publ., Dordrecht, The Netherlands, 249–285 (1987).

S11. Budd, W. F., Keage, P. L. & Blundy, N. A. Empirical studies of ice sliding. *J. Glaciol.* **23**(89), 157–170 (1979).

Table S1: Fitting equations, correlation coefficients (r), p-values and root mean square errors (σ) obtained by the regression analysis of air temperature (T in °C) and ice speed measured at GPS1 (u in m d^{-1}).

Period	Equation	r	p	σ
2008/09	$u = 0.048T + 0.90$	0.69	$< 10^{-6}$	0.119
2010	$u = 0.053T + 0.89$	0.77	$< 10^{-6}$	0.144
All	$u = 0.053T + 0.88$	0.76	$< 10^{-6}$	0.140

Table S2: Fitting equations, correlation coefficients, p-values and root mean square errors obtained by the regression analysis of the logarithms of effective pressure (P_e in MPa) (measured in BH1, BH2 and mean of the two boreholes) and ice speed (measured at GPS1 and GPS2) (u in m d^{-1}).

GPS1				
Borehole	Equation	r	p	σ
BH1	$u = 0.98P_e^{-0.34}$	-0.87	$< 10^{-6}$	0.063
BH2	$u = 1.05P_e^{-0.20}$	-0.62	$< 10^{-6}$	0.107
Mean	$u = 0.91P_e^{-0.35}$	-0.89	$< 10^{-6}$	0.061

GPS2				
Borehole	Equation	r	p	σ
BH1	$u = 0.55P_e^{-0.42}$	-0.91	$< 10^{-6}$	0.038
BH2	$u = 0.59P_e^{-0.26}$	-0.67	$< 10^{-6}$	0.074
Mean	$u = 0.50P_e^{-0.44}$	-0.93	$< 10^{-6}$	0.036

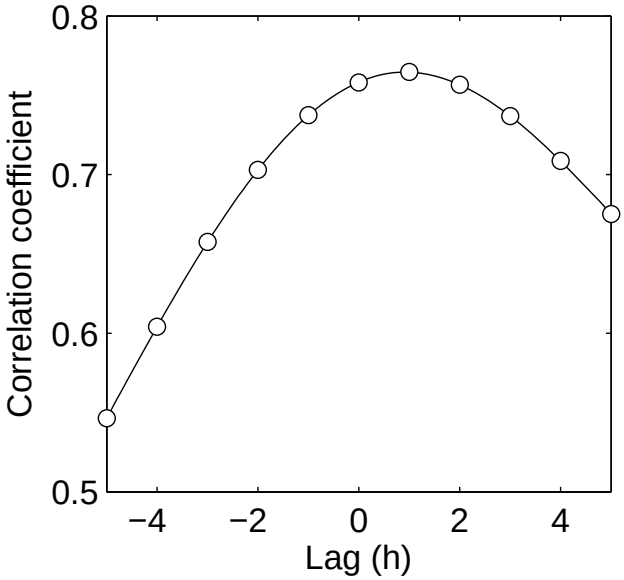

Fig. S1: Lagged correlation between ice speed at GPS1 and air temperature in 2008/09 and 2010 austral summer seasons. A positive lag denotes the lead of the air temperature.

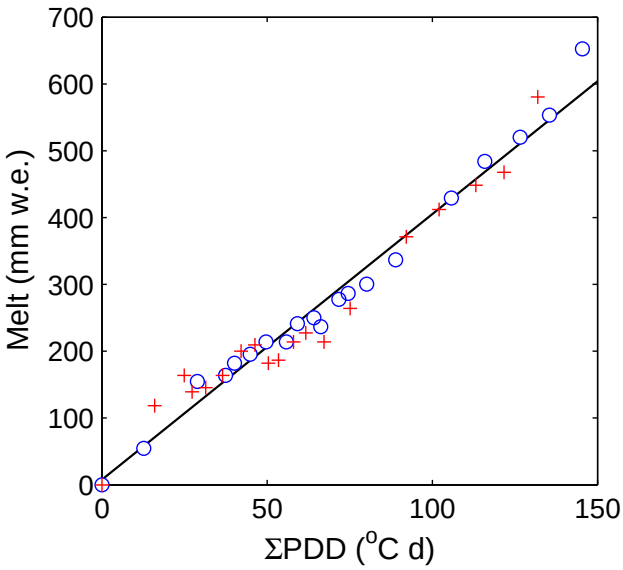

Fig. S2: Accumulated surface ice melt v.s. the sum of PDD at GPS1 (○) from 26 February to 12 March and at GPS2 (+) from 27 February to 12 March 2010. The regression line was obtained by the least square method.

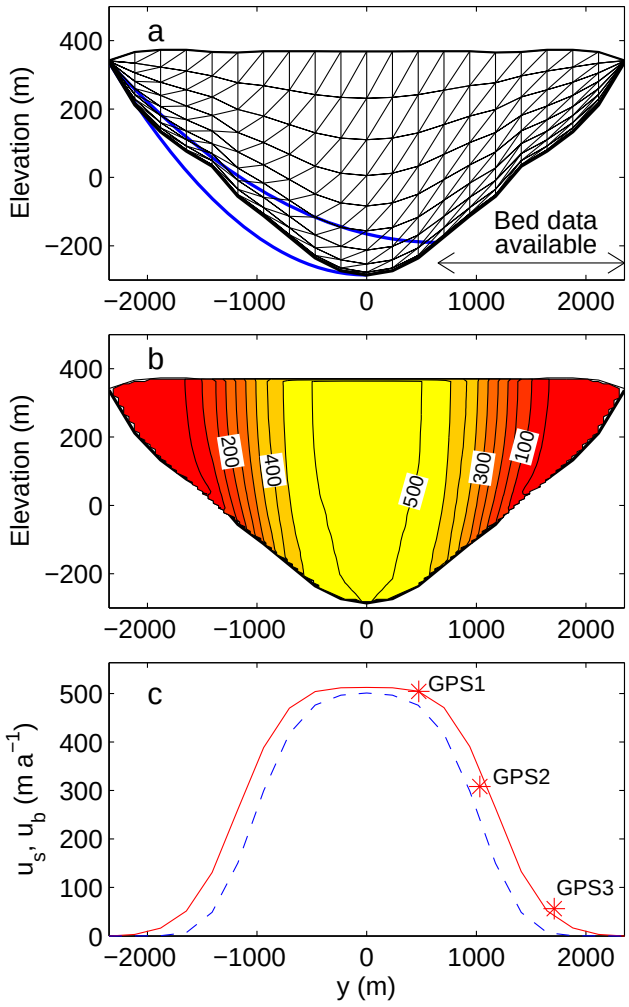

Fig. S3: Ice flow field computed with a two-dimensional ice flow model. (a) The transverse cross section of Glaciar Perito Moreno along the GPS profile and a finite-element mesh used for the numerical modelling. The blue curves are bed geometries used for the sensitivity study. (b) A computed horizontal ice speed field after tuning the basal boundary condition for the observed surface ice speed. The contour intervals are 50 m a^{-1}. (c) Surface (solid) and basal ice speed (dashed) as computed in (b) with mean surface ice speed ($*$) observed at GPS1–3 from 31 December 2008 to 7 January 2009.

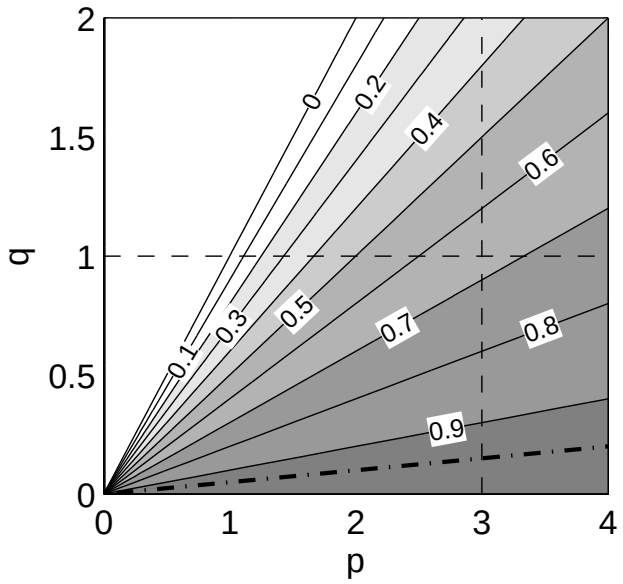

Fig. S4: Critical basal water pressure as a fraction to ice overburden pressure ($\frac{P_w}{P_i}$). Ice thickness dependence of the basal ice speed ($\frac{\partial u_b}{\partial h}$) is negative when the pressure is greater than the critical value. The dashed lines indicate commonly used values of p and q. The dash-dotted line corresponds to the water pressure observed in Glaciar Perito Moreno.